J Intell Robot Syst (2012) 68:373–386
DOI 10.1007/s10846-012-9766-6

Underwater Vehicle Localization with Complementary Filter: Performance Analysis in the Shallow Water Environment

Antonio Vasilijevic · Bruno Borovic · Zoran Vukic

Received: 17 January 2012 / Accepted: 6 August 2012 / Published online: 31 August 2012
© Springer Science+Business Media B.V. 2012

Abstract Rapid development of underwater technology during the last two decades yielded more affordable sensors and underwater vehicles, and, as a result, expanded their use from exclusively offshore industry towards smaller interdisciplinary research groups. Regardless of application, knowing the location of the vehicle operating underwater is crucial. Relatively inexpensive solution is sensor fusion based on a dynamic model of the vehicle aided by a Doppler Velocity Log and a Ultra-Short Base Line position system. Raw data from the sensors are highly asynchronous and susceptible to outliers, especially in shallow water environment. This paper presents detailed sensor analysis based on experimental data gathered in shallow waters, identifies outliers, presents an intuitive and simple sensor fusion algorithm and finally, discusses outlier rejection. The approach has been experimentally verified on medium size remotely operated vehicle.

A. Vasilijevic · B. Borovic (✉) · Z. Vukic
Faculty of Electrical Engineering and Computing,
Department of Control and Computer Engineering,
Laboratory for Underwater Systems and Technologies,
University of Zagreb, Unska 3, 10000 Zagreb, Croatia
e-mail: b_borovic@yahoo.co.uk

A. Vasilijevic
e-mail: antonio.vasilijevic@fer.hr

Z. Vukic
e-mail: zoran.vukic@fer.hr

Keywords USBL · DVL · Underwater localization · Underwater vehicle

1 Introduction

Where am I? The underwater robot leaves the ship and disappears into the sea. Once in the water, it cannot be seen anymore and an operator should rely solely on sensors to obtain its location. Accurate localization enables easier navigation, helps avoiding dangerous situations such as collision with ship, provides position feedback for the control algorithms and is a basis for subsequent smoothing algorithms used for accurate georeferencing. Good localization is required for all the underwater activity.

Unfortunately, a Global Positioning System (GPS) cannot be used for the underwater localization. Electromagnetic waves do not propagate well through the water causing the GPS to become practically useless. As a result, the underwater localization relies on inertial and especially, acoustic sensors. As accurate inertial navigation systems (INS) are extremely expensive, low cost applications are restricted to the use of attitude heading reference systems (AHRS). As the AHRS provide only accurate vehicle orientation, i.e. roll, pitch and yaw angles, with respect to the Earth reference frame, positioning itself is obtained through acoustic systems based on several

spatially distributed acoustic nodes. The distance between these nodes differentiates the type of the acoustic positioning systems. Typical examples are a long baseline (LBL), short baseline (SBL) and an ultra short baseline (USBL) system. The USBL system is characterized with the lowest accuracy, lowest acquisition cost and its easy deployment results in low-cost operations. On the other hand, the LBL system provides the highest accuracy but is more expensive to acquire and deploy. Besides providing position, the acoustic sensors are also used to measure velocity of the vehicle. Doppler Velocity Log (DVL) measures relative velocity over a bottom or a water column. Good overview of underwater navigation sensors is provided in [1].

Acoustic sensors are far from ideal. Both USBL and the DVL are susceptible to outliers, especially USBL in shallow waters. Bad alignment and inadequate calibration can result in unacceptably large errors. Proper preparation of sensors is therefore crucial for achieving specified performance. Furthermore, the USBL provides position measurements with bounded error at low data rate while DVL provides the velocity measurements at higher data rate. Although the subsequent integration of velocity provides smoother position estimate it suffers from drift. Nonetheless, it is possible to combine USBL and DVL outputs through a sensor fusion algorithms yielding an improved performance of the position estimate [2–8].

The objective of this paper is to present the experimentally verified localization scheme for the underwater vehicle. The approach includes analysis of the USBL and DVL sensors, intuitive and simple sensor fusion design and, finally, discussion on a three-level strategy for outlier rejection. At the end, the experimental results are provided and discussed before the final conclusions are given.

2 Sensor Performance Analysis

The localization approach described in this paper involves AHRS, pressure sensor, GPS, USBL and DVL. Together, they provide attitude, depth, position and linear velocities of the vehicle. AHRS, GPS and pressure sensor are only briefly described, while majority of the section focuses on the functionality, specifications, calibration and outliers associated with the acoustic sensors.

Magnetic compass is one of the most common sensors found in marine equipment. It usually comprises three magnetometers measuring the Earth's magnetic field. Both scale factor and offset of the sensor are affected by its pre-magnetization. Moreover, when compass is installed within the vehicle, the surrounding material, moving together with compass, distorts Earth's magnetic field around it and causes error called magnetic deviation. Theoretically, both types of error can be dealt with by calibration. In practice, however, the inadequately calibrated compass is a common source of problems. Furthermore, the magnetic compass has to be compensated for magnetic variation, which is the difference between true and magnetic North. Earth's magnetic field also contains a vertical, Z, component allowing three orthogonal magnetometers to act as an inclinometer, providing roll and pitch angles. Detailed discussion on magnetometers can be found in [9–11].

Magnetometers can be aided by three accelerometers and three angular rate sensors. Such multi-axis sensor assembly forms an IMU which, with addition of on-board processing system, becomes a AHRS. The accelerometers improve inclination functionality while angular rate sensors contribute to smoother attitude and faster sensor dynamics. Unlike traditional INS which provides both attitude and position, AHRS provide only estimate of attitude, i.e. roll, pitch and heading angle. In our application the AHRS can be found in the USBL, DVL and in the underwater vehicle itself.

Unlike magnetic, the depth and GPS measurements are not so problematic. Pressure sensors depend on reliable technology and it is only important to calibrate them properly. The offset is minimized at the sea level while the right scale factor is obtained from the subsequent dive at the known depth. In this paper, due to its reliability, the pressure sensor data is taken directly as a depth estimate, and is extensively used in outlier rejection scheme. On the other hand, the GPS does not require any calibration. The accuracy of the GPS used in experiments was ± 2 m. It is worth noticing that GPS sensor, after prolonged

inactivity, takes 10 to 20 s to acquire satellite data and converges to the specified accuracy.

2.1 USBL

USBL comprises a transducer attached to the platform and a transponder attached to the underwater vehicle (ROV) as shown in Fig. 1. Acoustic signal is emitted into the water and is received by a transponder. The transponder sends a response which arrives at four receivers $R0$–$R3$ embedded within the transducers head. Total signal travelling time and known speed of sound in the water determine the distance between the transducer and transponder, also called a slant range. The small differences of arrival times between the respective receivers allows for two angles, i.e. target azimuth and target elevation, to be determined. The position of the transponder in the transducer's frame of reference is then determined from these two angles and the slant range.

In order to get the absolute position of the transponder in North–East–Down (NED) reference frame [12] of the transducer, we need both absolute position and the attitude of the transducer. The absolute position of the transducer is determined from the position of the platform, measured by the GPS, and the distance, i.e. lever arms, between the GPS and the USBL transducer as shown in Fig. 1. For small ships where the lever arms are short and the GPS is close to the USBL transducer, it is enough to add the lever arms to the position measured by the GPS. Errors induced by neglecting the attitude of the ship are insignificant and do not affect USBL accuracy. For larger ships, however, where the lever arms can be longer, the attitude of the ship may induce errors and it has to be taken into account. Good material on the USBL systems is given in [13–15].

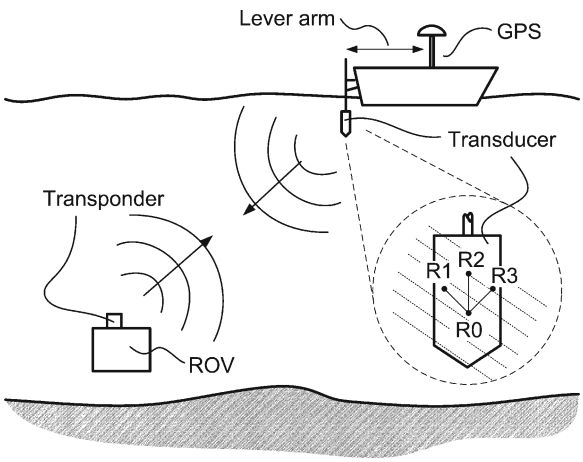

Fig. 1 Deployment and basic functionality of USBL

Specifications of the Tritech Micro Nav USBL used in the paper are: Tracking range: 500 m (typical horizontal), 150 m (typical vertical). Range accuracy is ±0.2 m, Bearing accuracy is ±3° and position update rate is 0.5–10 s. In order for the USBL to meet above specifications it is important to carefully set the system up and calibrate it. This involves compass calibration, alignments of reference frames, measurements of speed of sound and the lever arms. For example, only 1° of misalignment combined with a slant range of 100 m induces position error of 1.75 m. On the other hand, a 1 % error in the speed of sound measurement induces error of 1 m per 100 m of slant range. Some advanced USBLs use overall dynamic calibration, as explained in [16], where the procedure involves maneuvering the vessel around and over a stationary reference transponder on the seabed to determine the mounting offsets and the pitch, roll and heading corrections.

By neglecting the lever arm effect because the ship is small, the projection of the slant range, R, to the surface, i.e. X–Y plane, can be calculated as $R_{xy} = \sqrt{R^2 - Z^2}$. The R_{xy}, referring to Fig. 2, is used directly to determine the relative

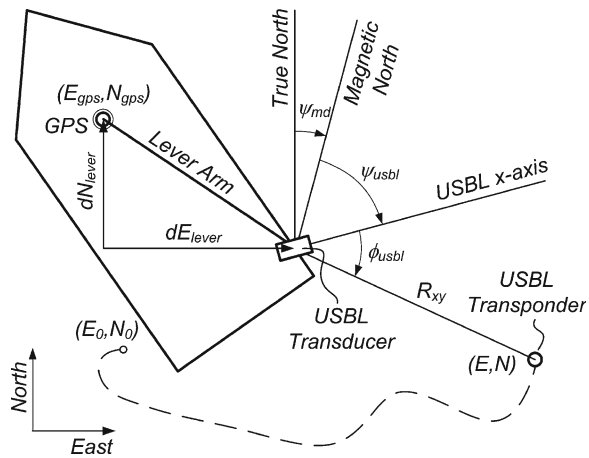

Fig. 2 Geometrical relations between the GPS and USBL transducer mounted on the ship and the USBL transponder

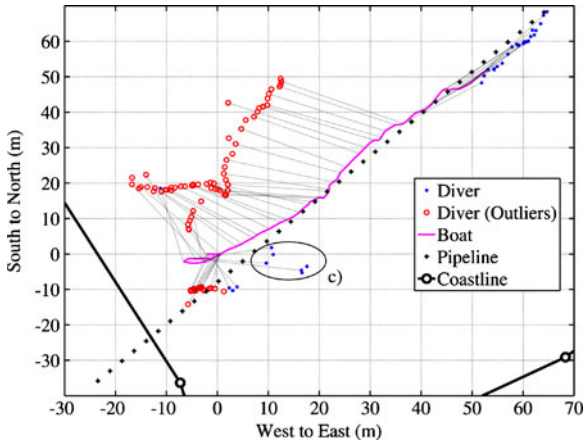

Fig. 3 Regular diver position (*dots*) and outliers (*circle*) caused by the reflection from the hull, shown in the XY plane with respect to the motion of the boat (*line*)

distance from the transponder to the transducer in northwards, $dN_{\text{usbl}} = R_{xy}\cos(\psi_{\text{usbl}} + \phi_{\text{usbl}} + \psi_{\text{md}})$, and the eastwards, $dE_{\text{usbl}} = R_{xy}\sin(\psi_{\text{usbl}} + \phi_{\text{usbl}} + \psi_{\text{md}})$, direction. Angle ψ_{usbl} is the USBL heading, ψ_{md} corrects magnetic variation and ϕ_{usbl} is the angle of incoming transponder sound relative to the heading.

Absolute position of the transponder in Earth's NED frame is given as

$$N = dN_{\text{usbl}} + N_{\text{gps}} + dN_{\text{lever}} \tag{1}$$

$$E = dE_{\text{usbl}} + E_{\text{gps}} + dE_{\text{lever}} \tag{2}$$

where N_{gps} and E_{gps} are absolute position measured by the GPS and dN_{lever} and dE_{lever} are projection of the lever arm in the NED reference system as shown in Fig. 2. Note that later, while using Eqs. 1 and 2 as an inputs to a filter, we actually transform the position coordinates into a "local reference frame" with origin in (E_0, N_0) for easier interpretation of results.

Unfortunately, the USBL system is susceptible to outliers due to the presence of acoustically reflecting surfaces within the operational environment. In order to illustrate typical outliers some experimental data is provided. The diver equipped with USBL transponder was following the rope marking the future route of the pipeline between the mainland and a nearby island. The boat equipped with the USBL transducer tracked the diver. The weather was calm, the maximal diver's depth along the transect was about 50 m.

Figures 3 and 4 illustrate several groups of outliers in X–Y plane and time domain, respectively. Group (a) is the beginning of the dive. The diver is just close to the surface and depth is slightly negative. Negative depth indicates that the reflection occurred above the transducer. Potential reflections from the surface and fact that diver may be above the transducer yields this data unreliable. Group (b) has irregular negative depth like the group (a), discontinuity in bearing data and do not have discontinuity in range. The bearing indicates that the acoustic beam hits the transducer

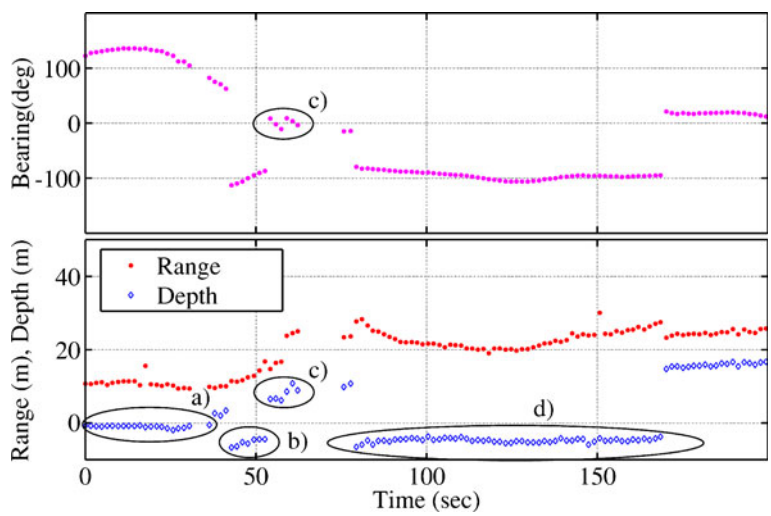

Fig. 4 Bearing (*dots top*), slant range (*dots bottom*) and depth (*diamonds bottom*) showing outliers caused by the reflection from the hull of the boat in the time domain

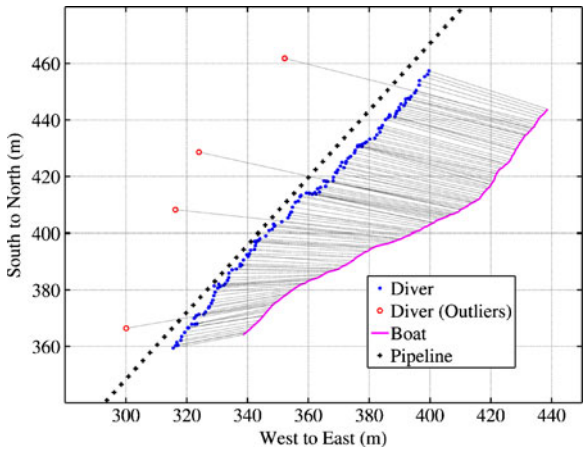

Fig. 5 Regular diver position (*dots*) and outliers (*circle*) caused by the reflection from the surface and bottom, shown in the XY plane with respect to the motion of the boat (*line*)

from the opposite side of diver's position. Finally, continuity of range indicates that the reflection occurs close to the transducer. Overall, these outliers seem to be reflections from the hull of the boat. Outliers under (d) are similar in nature but have discontinuity in range indicating additional reflection either from the surface or the bottom. Next, the observations denoted by (c) have positive depth but there is a 20° discontinuity in bearing between the first and second set of three observations. At least one of them is a set of outliers but it is not conclusive whether it is the first one, second one or both of them. It is likely, from Fig. 3, that three points closer to the pipeline are not outliers. Finally, two observations between regions (c) and (d) seem to be valid data but, as they stand as isolated data, it is ungrateful to evaluate them.

Figures 5 and 6 illustrates a group of outliers characterized by both slant range and depth being slightly less than two times of expected range and depth. As the increased slant range is a firm sign of reflection, the double range indicates the double reflection, i.e. the reflection from both the surface and the bottom. Also, it is obvious that bearing is not affected when the outlier occurs, indicating that the reflection occurred for the primary beam, i.e. the one travelling from the transducer to the transponder.

2.2 DVL

DVL comprises four directional transducers, each of them capable of transmitting and receiving sound. Transducers are deployed 90° from each other around the vertical axis of the sensor. Transducers form a substantially small angle with vertical axis as shown in Fig. 7.

The sound is transmitted from each of the four beams at frequency f. The sound bounces off the bottom or water column and comes back with frequency shift proportional to relative velocity due to the Doppler effect. Three linear velocities, u', v' and w' with respect to the x, y and z axis of the sensor, are determined from four frequency

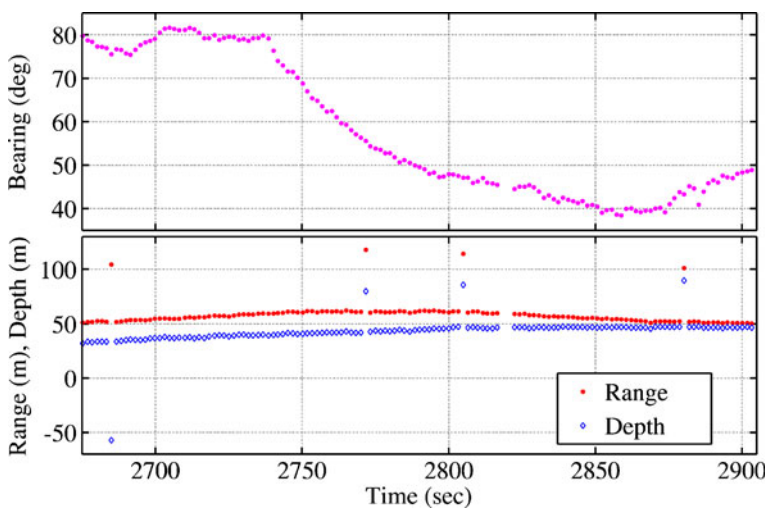

Fig. 6 Bearing (*dots top*), slant range (*dots bottom*) and depth (*diamonds bottom*) showing outliers caused by the reflection from the surface and bottom in the time domain

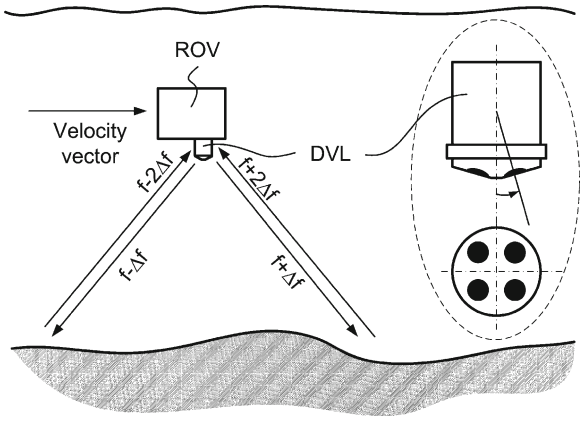

Fig. 7 Typical DVL sensor with four transducers deployed 90° from each other around the vertical axis

shifts. Besides velocity data, the DVL calculates and provides an altitude above the bottom.

The DVL sensors are typically enhanced with an AHRS in order to correct vehicle velocities for roll and pitch, and transform the velocity vector from sensor to Earth's reference frame. Corrected velocities are given as [12]: $[u\, v\, w]' = \mathbf{C}[u'\, v'\, w']'$ with elements of matrix $\mathbf{C}$ given as: $C_{11} = \cos\theta$, $C_{12} = \sin\theta \sin\phi$, $C_{13} = \sin\theta \cos\phi$, $C_{21} = 0$, $C_{22} = \cos\phi$, $C_{23} = -\sin\phi$, $C_{31} = -\sin\theta$, $C_{32} = \cos\theta \sin\phi$, $C_{33} = \cos\theta \cos\phi$, where ϕ is roll angle and θ is pitch angle provided by the AHRS within the DVL.

Operating frequency for the NavQuest 600P Micro DVL used in this paper is 600 kHz, accuracy is 1 mm/s plus 0.2 % of actual velocity, minimum and maximum operating altitudes are 0.3 and 110 m, respectively, maximum velocity is 20 kts, and highest update rate is 0.2 s. In addition, the DVL provides information on whether measurement was obtained through the bottom or the water lock. Good reference on DVL is given in [17].

For example, velocity of 0.5 m/s induces offset of 1 mm/s + 0.2 % of 0.5 m/s totaling 2 mm/s. This offset induces error of 7 m after 1 h. Much larger error may occur when the DVL is physically misaligned with the robot reference frame or when the compass is not calibrated properly. Only 1 deg of misalignment, coupled with velocity of 0.5 m/s causes lateral error of 30 m after 1 h. Finally, the velocity measurement is directly proportional to the speed of sound. For example, 1 % or 15 m/s error in speed of sound, coupled with robot velocity of 0.5 m/s adds up to 18 m after 1 h.

DVL is also susceptible to outliers. First, when water lock occurs, our experience shows it is unreliable measurement and it is advisable to reject it. Another type of outlier is illustrated in Fig. 8 where majority of velocity measurements are wrong for altitudes less than 0.6 m. The problem is present at smaller scale for altitudes up to 3 m.

2.3 Underwater Vehicle Dynamics

The model of the underwater vehicle is based on rigid body motion and has a quite complex, nonlinear and coupled multi-degree of freedom (DOF) dynamics [18–20] and is given as

$$\mathbf{M}\dot{\boldsymbol{\nu}} + \mathbf{C}(\boldsymbol{\nu})\boldsymbol{\nu} + \mathbf{D}(\boldsymbol{\nu})\boldsymbol{\nu} + \mathbf{g}(\boldsymbol{\eta}) = \boldsymbol{\tau} + \mathbf{g_o} + \mathbf{w} \qquad (3)$$

where $\mathbf{M}$ is the 6×6 system inertia matrix including added mass, $\mathbf{C}(\boldsymbol{\nu})$ is the 6×6 Coriolis-centripetal matrix including added mass, $\mathbf{D}(\boldsymbol{\nu})$ is 6×6 damping matrix, $\mathbf{g}(\boldsymbol{\eta})$ is the 6×1 vector of gravitational / buoyancy forces and moments,

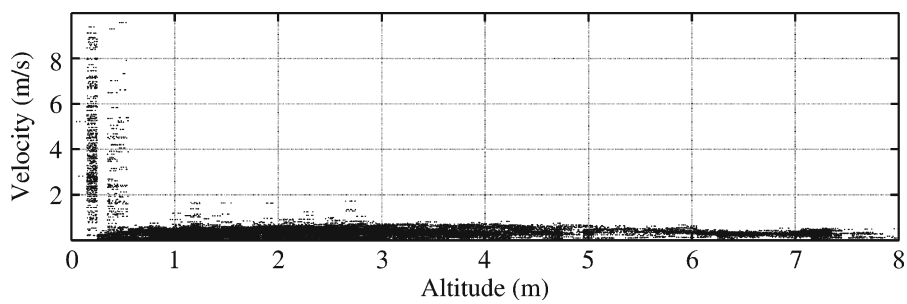

Fig. 8 Unreliable velocity measurements at low DVL altitude taken for actual velocities strictly limited to 0.4 m/s

$\boldsymbol{\tau}$ is the 6×1 vector of control inputs, $\mathbf{g_o}$ is the 6×1 vector used for predetermining (ballast control), $\mathbf{w}$ is the 6×1 vector of environmental disturbances, $\boldsymbol{\nu}$ is the 6×1 velocity vector and $\boldsymbol{\eta}$ is the 6×1 position and orientation vector in surge, sway, heave, roll, pitch and yaw degrees of freedom (DOF). Matrices $\mathbf{M}$, $\mathbf{C}$ and $\mathbf{D}$ have off diagonal elements implying that the different DOFs are coupled. Also, elements of $\mathbf{C}(\boldsymbol{\nu})$, $\mathbf{D}(\boldsymbol{\nu})$ and $\mathbf{g}(\boldsymbol{\eta})$ are generally nonlinear.

At first, the dynamical modeling does not seem to fit into the sensor section. However, it belongs to sensor system and is regularly used to assist sensor fusion especially as an integral part of observer for underwater vehicle navigation [18, 21, 22]. The dynamical model improves the performance and reliability of the observer, because the estimate of the position does not rely on pure kinematics, i.e. on USBL readings combined with direct integration of DVL data.

However, poorly formulated models that does not capture the important characteristics of the dynamic system, may cause reduced performance and also stability problems when used in the closed loop control [22]. It is always better to include more complete model in order to capture couplings, nonlinearities and external disturbances. The choice of the model has a significant impact on a position estimate. Unfortunately, as the model gets more complex, its identification gets more complicated, time consuming and more expensive to obtain. In addition, the use of some underwater vehicles is often very flexible, a payload frequently changes and, consequently, the dynamics is significantly altered. This presents additional burden on keeping the accuracy of complex dynamical models. Typically, the complexity of the model is adjusted according to application and required accuracy.

The simplest approach to sensor fusion presented in this paper would be application of a pure kinematic model. However, the possibility of prolonged data outages requires having at least the simplest form of the dynamical model. On the other hand, the localization in a horizontal plane, i.e. surge, sway and yaw DOFs, is of primary interest. Generally, for a slowly moving vehicle with small magnitudes of roll and pitch, vertical motion is uncoupled from horizontal motion and can be dropped out, resulting in reducing Eq. 3 to three coupled and nonlinear DOF describing horizontal dynamics. Identification of coupling and nonlinear parameters was not done due to the lack of resources needed to perform this relatively complex procedure, limiting the application to the use of uncoupled and linear three DOF model. The fact that the model is used only for localization and not for closed loop control may, up to some point, justify such severe simplification of the model. Furthermore, as the heading measurement is reliable and readily available with relatively low noise, i.e. 0.2°_{rms}, it was decided to avoid additional filtering. The Eq. 3 is therefore reduced to surge and sway DOFs only.

Besides control forces, the underwater vehicle is subject to external forces such as sea current and vehicle's tether. The common assumption in modeling of the sea current is that it is constant or slowly varying [18, 22]. This assumptions becomes questionable in shallow water environment where the underwater vehicle is operated from a coast or a boat anchored close to the coast. Rugged coastline and vehicle position relative to it may cause current to change rapidly both its direction and intensity. To make things worse, unlike in deep water operations where tether is vertical, in shallow water environment the tether is extended more or less horizontally. Hence, tether disturbances are coupled to the vehicle position, fickle sea current as well as to the actions of a tether operator. As a result, the external disturbances can have both low and high frequency components making it tough to model external disturbances accurately, and especially to extract external disturbances from thruster inputs. Consequently, there are two options. Either to include the model of external disturbances which, with its complexity in tether modeling and inconsistency in sea current direction and intensity, do not leave us with a lot of confidence in its accuracy or, on the other hand, to simply exclude it. In both cases prolonged DVL and USBL outages may cause the localization error to drift away. In this paper, as the model is used only for localization and not for closed loop control, the simple and application-sufficient linear two DOF model without external disturbances was implemented.

Based on the discussion above, the resulting model is given as

$$m\dot{u}_m = k_\tau \tau_u - b_u u_m \tag{4}$$

$$m\dot{v}_m = -b_v v_m \tag{5}$$

where u_m and v_m are modeled surge and sway velocities in vehicle-fixed frame, τ_u represents thrust in surge DOF given in % of full scale, b_u and b_v are the viscous damping coefficients in surge and sway DOFs, k_u is thruster gain in surge DOF, m represents mass and added masses of the vehicle [12]. Parameters of the model are $k_u = 0.038$ N/%, $b_u = 6$ kg/s, $b_v = 18$ kg/s and $m = 30$ kg.

3 Sensor Fusion Filter Design

The USBL provides position measurements at low data rate and with bounded error while the DVL runs at higher data rate and provides smoother but drift-susceptible position estimate based on integration of its velocity measurements. Generally, both sensors generate asynchronous stream of data so the dynamic model is introduced to upsample data at the sensor fusion rate. The purpose of this section is to build a filter fusing the best from each of these three data sources (USBL, DVL and the dynamic model) and provide a high-performance position estimate.

The most common approach to the sensor fusion is Kalman filtering. Extended Kalman Filter (EKF), characterized with nonlinear system model, has been applied in large number of ship and underwater vehicle applications, e.g. [23]. One drawback of the EKF is that kinematic and kinetic equations must be linearized about varying velocities and a yaw angle. Also, when used as a part of the closed loop system, only local exponential stability is ensured [18]. In addition, tuning of Kalman filters is difficult and time consuming because it is a stochastic system with large number of states and covariance equations [18]. Most of these parameters are non-intuitive and difficult to relate to physical quantities. These problems motivate the search for a easy-to-tune nonlinear fixed gain observer which covers the whole state space and is Globally Asymptotic Stable (GES)—a nonlinear passive observers.

Nonlinear passive observers were introduced into navigation during the last decade, e.g. [24]. An example for underwater application is given in [21]. Passive nonlinear observers are derived in deterministic setting but can be used in stochastic systems. The structure of the passive observer is essentially full nonlinear model of the vehicle, including various disturbances. After the model is established, the fixed observer gains are chosen such that the error dynamics is GES [24].

The approach presented in this paper is a simple complementary sensor fusion filter with highly intuitive insight into its functionality. It resembles the structure of nonlinear passive observer. It is nonlinear in kinematic equations and has fixed gains. Actually, if two filters are compared the structure of the complementary filter is simply an incomplete version of the structure of the nonlinear passive observer.

3.1 DVL-Aided Surge Velocity Model

In continuous time domain, the simple aiding of the surge 4 and sway 5 with the DVL measurements, u and v, yields

$$\dot{\hat{u}}_m = (1/m)[k_\tau \tau_u - b_u \hat{u}_m + k_{fu}(u - \hat{u}_m)] \tag{6}$$

$$\dot{\hat{v}}_m = (1/m)[-b_v \hat{v}_m + k_{fv}(v - \hat{v}_m)] \tag{7}$$

where $\hat{u}_m$ and $\hat{v}_m$ are estimated surge and sway velocities while k_{fu} and k_{fv} are filter gains.

However, the DVL data is generally asynchronous and therefore, before discretization of Eqs. 6 and 7, it is necessary to fill in, or upsample the DVL measurements with model outputs. This is done in the way that Eqs. 4 and 5 are discretized with $d/dt = (q-1)/h$

$$\bar{u}_{m,k+1} = (hk_\tau \tau_{u,k} + k_{mbu}\bar{u}_{m,k})/m \tag{8}$$

$$\bar{v}_{m,k+1} = k_{mbv}\bar{v}_{m,k}/m \tag{9}$$

where $k_{mbu} = m - hb_u$, $k_{mbv} = m - hb_v$, h is a sampling time, q is a forward shift operator and subscript k defines a discrete system. The model states, $\bar{u}_{m,k}$ and $\bar{v}_{m,k}$, are updated as $\bar{u}_{m,k} = u(t_{\mathrm{DVL}})$ and $\bar{v}_{m,k} = v(t_{\mathrm{DVL}})$ at the new DVL acquisition instance, t_{DVL}. Consequently, $\bar{u}_m$ and $\bar{v}_m$, which are now upsampled and synchronized with sampling, becomes the discrete version of the

DVL measurement u. Subsequent discretization of Eqs. 6 and 7 yields

$$\hat{u}_{m,k+1} = (hk_\tau \tau_{u,k} + k_{mbu}\hat{u}_{m,k} + hk_{fu}e_{um,k})/m \tag{10}$$

$$\hat{v}_{m,k+1} = (k_{mbv}\hat{v}_{m,k} + hk_{fv}e_{vm,k})/m \tag{11}$$

where $e_{um,k} = \bar{u}_{m,k} - \hat{u}_{m,k}$, $e_{vm,k} = \bar{v}_{m,k} - \hat{v}_{m,k}$, k_{fu} and k_{fv} are filter gains. In our case $k_{fu} = 50$ kg/s, $k_{fv} = 50$ kg/s and $h = 0.1$ s.

3.2 Position-Aided Velocity Filter

The USBL and DVL-aided velocity model data are fused through a simple complementary filter [25] as shown in Fig. 9. Inputs to the filter are velocities from the dynamic model 10 and 11, $\hat{u}_m$ and $\hat{v}_m$, the USBL measurement Eqs. 1 and 2, and heading ψ. Outputs are position estimates $\hat{N}$ and $\hat{E}$. The estimated velocities, $\hat{u}$ and $\hat{v}$, are transformed from the body-fixed reference frame to the Earth-fixed reference frame. Integrator integrates transformed velocities, $\dot{\hat{u}}$ and $\dot{\hat{v}}$ in order to estimate position. Position error is obtained through comparison of the position estimate and USBL measurement and is transformed back to the body-fixed reference frame. The transformed error is filtered through the filter comprising adjustable parameters k_u, k_v and an integrator.

Both DVL and USBL measurements contain actual value of the signal, band-limited white noise and the measurement bias. Integrated DVL bias represents drift in the position estimate. Assume, in Fig. 9, that the $\psi = 0$ and $\hat{v} = 0$, hence yielding the position estimate $\hat{N} = k_u/(s + k_u)N + \hat{u}_m/(s + k_u)$. The bias within $\hat{u}_m$ is constant, i.e. $s = 0$ so the estimation error due to DVL bias is bounded to $\hat{u}_m/k_u$. Assuming relatively large bias of 5 mm/s and $k_u = 0.1s^{-1}$ the estimated position error is negligible, i.e. 5 cm. Effectively, the DVL output is high pass filtered through $G_{\mathrm{HP}} = s/(s + k_u)$ and the USBL signal is effectively low-pass filtered through $G_{\mathrm{LP}} = k_u/(s + k_u)$. There is no loss of information because $G_{\mathrm{LP}} + G_{\mathrm{HP}} = 1$.

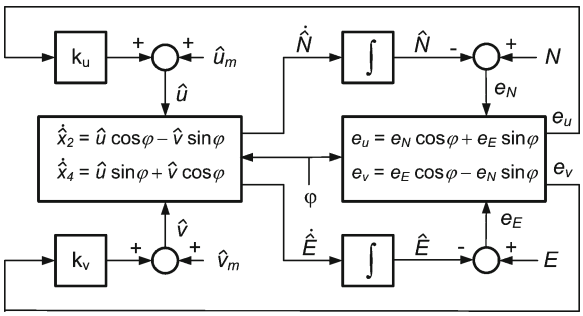

Fig. 9 Complementary filter with USBL-aided DVL position estimate

The discrete version of the filter is given as

$$e_{N,k} = \bar{N}_k - \hat{N}_k \tag{12}$$

$$e_{E,k} = \bar{E}_k - \hat{E}_k \tag{13}$$

$$e_{u,k} = e_{N,k}\cos\psi_k + e_{E,k}\sin\psi_k$$

$$e_{v,k} = e_{E,k}\cos\psi_k - e_{N,k}\sin\psi_k$$

$$\hat{u}_k = k_{u,k}e_{u,k} + \hat{u}_{m,k} \tag{14}$$

$$\hat{v}_k = k_{v,k}e_{v,k} + \hat{v}_{m,k} \tag{15}$$

$$\hat{N}_{k+1} = \hat{N}_k + h(\hat{u}_k\cos\psi_k - \hat{v}_k\sin\psi_k)$$

$$\hat{E}_{k+1} = \hat{E}_k + h(\hat{u}_k\sin\psi_k + \hat{v}_k\cos\psi_k)$$

where $\hat{N}$ and $\hat{E}$ are position estimate in northwards and eastwards directions, respectively. Errors 12 and 13 are errors between upsampled USBL measurement and estimated position. The upsampled USBL measurements are obtained by integrating $\hat{u}_{m,k}$ and $\hat{v}_{m,k}$ as

$$\bar{N}_{k+1} = \bar{N}_k + h(\hat{u}_{m,k}\cos\psi_k - \hat{v}_{m,k}\sin\psi_k)$$

$$\bar{E}_{k+1} = \bar{E}_k + h(\hat{u}_{m,k}\sin\psi_k + \hat{v}_{m,k}\cos\psi_k)$$

When new USBL measurement arrives at time, t_{USBL} as shown in Fig. 10, $\bar{N}_k$ and $\bar{E}_k$ are updated

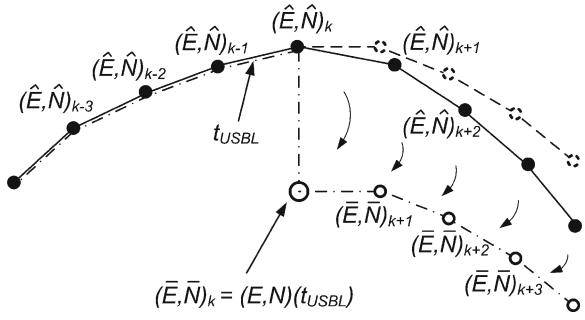

Fig. 10 Acquisition of the USBL data (*large hollow circle*) disrupts upsampled USBL measurement (*small hollow circle with dash-dot line*) and generates reference for position estimate (*filled circle with line*)

to $\bar{N}_k = N(t_{\mathrm{USBL}})$ and $\bar{E}_k = E(t_{\mathrm{USBL}})$, and filter parameters k_u and k_v in Eqs. 14 and 15 are reset at their initial value k_{u0} and k_{v0}. They decay exponentially as $k_{k+1} = k_k(T-h)/T$ until new USBL measurement arrives. Filter parameters are $k_{u0} = k_{v0} = 0.1\ \mathrm{s}^{-1}$ and $T = 0.5$ s. When USBL signal is absent for some time the estimates $\hat{N}$ and $\hat{E}$ converge towards $\bar{N}_k$ and $\bar{E}_k$, respectively.

3.3 Outlier Rejection Discussion

In metrology, an outlier is measurement that is numerically distant from the rest of the data. As such, outliers may seriously compromise the quality of the underwater position estimate [26] and have to be rejected. Typical approach to outlier detection would be a combination of filtering with change detector [27, 28], a technique well known from the adaptive filtering and fault detection. Filtering provides a residual of the signal, e.g. noise, which is fed into the change detector. From a change detection point of view, it does not matter which filter we use and modeling phase can be seen as a standard task [27]. Used filters can be, for instance, Recursive Least Squares (RLS) or Kalman filter.

The purpose of the change detector is to determine and average a distance measure to get a suitable test statistics which is then thresholded to determine whether the change occurred or not [27]. Change occurs if residual parameters, e.g. mean or variance, become "large" in some sense. The main problem in statistical change detection is to decide what "large" is. The outlier rejection is always a compromise between detecting true changes and avoiding false alarms.

One of the most commonly used change detectors is cumulative sum (CUMSUM) [27, 29], originally developed for production quality control. CUMSUM is based on calculation of cumulative sum of the logarithm of the likelihood (log-likelihood) ratio of residual's scalar parameters, e.g. mean or variance. Interquartile range is an another example of change detector where outliers are classified based on a their distance from a lower and upper quartiles of a set of data. An overview of change detectors can be found for instance in [29] or [27].

There are three typical approaches to change detection [27], one filter, two filters, and multiple-filter approach. For example, a RLS filter can be combined with CUMSUM detector resulting in RLS CUMSUM filter. Two filter approach combines slow and fast filter, e.g. compares a small set of recent data to a whole set of data, and uses likelihood approach to determine distance measure. General likelihood ratio (GLR) is a popular method based on two filter approach. Finally, the idea of multiple-model approach is to enumerate all conceivable change hypotheses and choose one which has the lowest residual.

In our application the main source of outliers are USBL and DVL. Especially annoying are outliers caused by multiple acoustic paths described in Section 2.1 and also reported, for instance, in [26, 30–32]. The systematization of the outliers in this paper is based on three criteria, (1) whether particular measurement is possible for a particular sensor, (2) whether particular measurement follows the trend in residual for single sensor and (3) whether relationship between the data from two or more sensors satisfies specified static or/and dynamic conditions. If measurement do not pass all three conditions it is treated as an outlier. Note that the approaches (2) and (3) are based on filter/change detector structure.

In the first approach the outliers are rejected by taking out signals which make no sense itself. For example, the value of the observation can be outside predetermined limits. The DVL velocity measurements shown in Fig. 8 are not reliable for altitudes below 0.6 m and are directly eliminated. Furthermore, the vehicle's velocities in x, y and z directions are limited by application. For example, the surge velocity of the vehicle is limited to 0.5 m/s in forward direction and to 0.3 m/s in backwards direction. Next, the USBL data is rejected if calculated depth is negative (see Fig. 6). In addition, as the USBL works more reliably when the transponder is more "below" than "away" from the transducer, the measurements can be rejected by setting a limit on a low depth-to-slant-range ratio.

In the second approach the single sensor signal which make no sense with respect to neighboring signals in the time domain are rejected as a outlier.

In our case, the approach can be used if there is not prolonged outages of USBL signal as shown, for example, in Figs. 5 and 6. The continuous sequence of USBL measurements is suddenly interrupted with a measurement that is substantially different (see Fig. 10). If $(\bar{E}, \bar{N})_k$ does not fit within the specified region around $(\hat{E}, \hat{N})_k$ the measurement is rejected. The difference between $(\hat{E}, \hat{N})_k$ and $(\bar{E}, \bar{N})_k$ can be seen as a residual. A single sensor approach for outlier rejection is described in [33]. The filter is based on causal moving data window, and is therefore fast and appropriate for real-time applications.

Similarly, the residual $e_{m,k}$ from Eq. 10 is "small" for several DVL measurements within last few seconds. If new DVL measurement increases the error $e_{m,k}$ above the threshold, i.e. the noise level for the DVL, the measurement is an outlier. The noise level condition can be expanded through the limits for expected velocity, $\bar{u}_{m,k}$. If $\bar{u}_{m,k}$ is not within $\hat{u}_{m,k} \pm \hat{u}_{lim,k}$ the measurement is rejected. Limits $\hat{u}_{lim,k}$ are determined from noise level, the accuracy of velocity model and dynamic conditions on surge velocity signal.

One could argue that it would be too conservative to exclude the DVL measurements in the above example if the estimation error that they produce is too big. Namely, the observer uses both the DVL and the USBL data and the big estimation error may be due to a problem in the USBL measurement that influences the velocity estimations as well, while the DVL is nicely working. Comparing the information from the various sensors will indeed help and is therefore addressed next. However, single sensor outlier rejection has an advantage of being quite intuitive and its conservative nature can be fine tuned to fit well with outlier rejection methods based on plurality of sensors.

The method belonging to the third approach which is used in this paper is the simple outlier rejection based on difference between the reliable depth measurement provided by the pressure sensor and the outlier-susceptible depth measurement provided by the USBL. There are numerous other examples involving simple relations between multiple sensors addressed elsewhere in the literature. In [30] each conceivable acoustic reflection is modeled and the outliers are essentially classified based on the model with minimal residual. In [31], for example, the outlier rejection is tied to the signal describing propeller activity, i.e. cavitation.

The approach, however, may include more complex rejection schemes. For example, a new USBL measurement can be evaluated against a region surrounding the present position estimate which was obtained by integration of the velocity of the vehicle since the last reliable USBL measurement. Due to the drift caused by DVL-aided model, the region in the X–Y plane containing the potential position grows larger with time, somewhat similar to covariance matrix in Kalman filter. When new USBL measurement arrives and falls outside the region, it is considered to be an outlier and is not processed by the fusion filter. Above procedure is applicable even for prolonged outages of the USBL signal. Similar approaches can be found elsewhere. In [32] Kalman filter integrates dead reckoning with the array of pre-deployed acoustic beacons and outliers are rejected through the time of arrival for each beacon. Position error is propagated and position uncertainty is transformed into uncertainty in predicted travel time and outliers are thresholded using the Mahalanobis distance. In [31] a new measurement is evaluated through its reasonableness by checking the Euclidian distance which depends on the time of last USBL hit. In [34], diffusion based observers process the whole segments of trajectory at the time allowing the consideration of important practical issues such as outliers in a simple framework. Diffusion term is interesting, for example, in cases where the noise in not Gaussian or to explicitly incorporate outliers into the filtering process.

In conclusion, the outlier rejection can be done in many ways, ranging from simple sensor cross-checks to complex filter-based algorithms. The outlier rejection is always a compromise. There is a point where rejection of too many observations become counter-productive and the localization works worse than without outlier rejection. The designer's, and especially user's objective is adjusting the rejection scheme, tightly tied to in-field conditions, close to this optimal point. The

intuitive nature of the algorithm greatly simplifies this task.

4 Experimental Results

Experiments were performed with Seamor 300F remotely operated vehicle (ROV) shown in Fig. 11. Maximum operating depth is 300 m and maximum speed is 3 kt, or around 1.5 m/s. The ROV dimensions are 472 × 355 × 355 mm and its weight is around 30 kg. The ROV propulsion comprises two horizontal and two vertical thrusters rated at 150 W and capable of producing 5 kg of thrust each. The horizontal propulsors allow for surge and yaw thrust and control while vertical thrusters allow for depth and lateral motion up to some level. The ROV is equipped with forward looking color CCD camera with manual/auto focus and 2 × 50 W LED lights, both mounted on a tilt platform. Furthermore, the ROV is equipped with DVL and USBL transponder described in Section 2.

In order to evaluate the sensor fusion filter, two sets of experimental results are provided illustrating the performance of the filter with and without USBL data. The mission was performed from the ship anchored close to a small island. The mission was defined with several straight lines the operator needed to follow. They were defined by desired heading, desired velocity and desired time. The results shown in Fig. 12 show that the filter performs well when USBL data is taken into account. However, when DVL-aided surge model is used, the offset builds up ending up in inaccurate position estimate.

Fig. 11 Seamor 300F remotely operated vehicle (ROV)

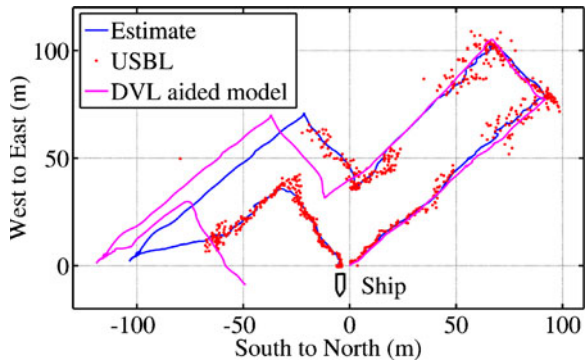

Fig. 12 Position estimate (*line*) in X–Y plane behaves well with the USBL aid (*dot*) but show large error if only DVL-aided model (*line*) is used

Next, the sensor fusion filter was evaluated against its accuracy, the polygon comprising three lines and four points was created. Three expandable ropes were stretched at the bottom between four points. The length of straight lines between the polygon were 91, 30 and 105 m, respectively. Each points was fixed with an anchor and a buoy, and its position was taken by GPS with $\sigma = 2m$ accuracy. The vehicle was piloted along these lines by following the ropes on video camera as shown in Fig. 13. Although positioning error can be determined only when the vehicle reaches anchoring points, the deflection from the desired trajectory can be determined in any moment. The results are shown in Fig. 14.

Fig. 13 Camera view from the ROV during the polygon-following mission

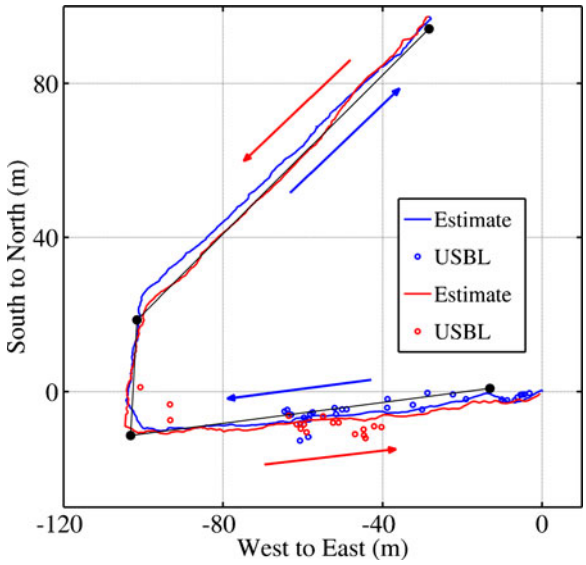

Fig. 14 The quality of position estimate (*line*) in X–Y plane with USBL-aiding (*circle*) verified over a polygon (*filled circle with line*)

5 Discussion

The first portion of the sensor fusion that was gradually and intuitively developed in Section 3 includes simple and relatively inaccurate dynamic velocity model. This simple model is important because it upsamples the DVL signal by the data obtained from the model 8 and synchronizes it with the sampling instances. The DVL measurements can be asynchronous either due to presence of invalid measurement or the measurement stamped as an outlier. In addition, the filter based on the velocity model 10 reduces DVL noise. Accuracy of the estimate depends on the accuracy of the DVL.

However, in order to estimate the position, the resulting velocities have to be transformed into the Earth fixed reference frame and subsequently integrated. Although the positioning error is caused mainly by the noise and outliers, it can be caused by inadequate preparation of sensors. For instance, the heading of uncalibrated compass, uncalibrated DVL offset or misalignment between compass and DVL reference frames can induce a large position error, as shown in Fig. 12. Therefore, sensor preparation and calibration need to be done meticulously.

Luckily, the error shown in Fig. 12 is corrected by the the USBL, which provides absolute position. Like the DVL data, asynchronous USBL data is synchronized to the 0.1 s rate through the upsampler that expands the USBL signal with the position estimates obtained from the velocity filter as shown in Fig. 10. The USBL is characterized with high noise content or abundance of outliers, as shown in Figs. 3, 5, 12 and 14 and these issues are addressed with data fusion and outlier rejection, respectively. The resulting position estimate, shown in Figs. 12 and 14, is continuous, low noise and accurate within the boundary of USBL accuracy.

In order to implement a well-performing practical filter, the performance of USBL and DVL sensors were analyzed with respect to the circumstances when outliers can occur. The filter itself provides a good platform for implementation of outlier rejection scheme due to its simplicity and intuitiveness. It is important to reject as many outliers as possible before data gets into the filter. Outliers are rejected through three criteria. These criteria are static sensor rejection clauses, dynamic sensor clauses, and clauses related to combination between signals from different sensors. Again, the outlier rejection is separated from filtering and occurs asynchronously, in a discretization step following the new measurement arrival.

6 Conclusions

This paper presents practical issues and procedures related to design of the fusion filter aimed at localization of underwater vehicles in the shallow water environment. The simple and yet well performed data fusion filter design is provided in tutorial-like fashion. Experimental results are accurate and show robustness of the approach even in the case some sensor data is missing or is contaminated with high noise. Special attention is paid to performance of the USBL and DVL sensors, associated outliers and their rejection. Although the provided data fusion performs well it is necessary to emphasize the significance of sensor preparation and calibration.

Acknowledgements The work was carried out in the framework of a Coordination and Support Action type of project supported by European Commission under the Seventh Framework Programme "CURE—Developing Croatian Underwater Robotics Research Potential" SP-4 Capacities (call EU FP7-REGPOT-2008-1) under grant agreement 229553.

References

1. Kinsey, J.C., Eustice, R.M., Whitcomb, L.L.: A survey of underwater vehicle navigation: recent advances and new challenges. In: Proc MCMC20067th IFAC Conference on Manoeuvring and Control of Marine Vehicles, Lisbon, Portugal, Invited paper (2006)
2. Miller, P., Farrell, J., Zhao, Y., Djapic, V.: Autonomous underwater vehicle navigation. IEEE J. Oceanic Eng. **35**(3), 663–678 (2010)
3. Hegrenaes, O., Hallingstad, O.: Model-aided ins with sea current estimation for robust underwater navigation. IEEE J. Oceanic Eng. **36**(2), 316–337 (2011)
4. Lee, P.-M., Jun, B.-H., Kim, K., Lee, J., Aoki, T., Hyakudome, T.: Simulation of an inertial acoustic navigation system with range aiding for an autonomous underwater vehicle. IEEE J. Oceanic Eng. **32**(2), 327–345 (2007)
5. Willumsen, A., Hallingstad, O., Jalving, B.: Integration of range, bearing and doppler measurements from transponders into underwater vehicle navigation systems. In: OCEANS 2006, pp. 1–6 (2006)
6. Jalving, B., Gade, K., Hagen, O., Vestgard, K.: A toolbox of aiding techniques for the hugin auv integrated inertial navigation system. In: OCEANS 2003. Proceedings, vol. 2, pp. 1146–1153 (2003)
7. Hegrenaes, O., Berglund, E., Hallingstad, O.: Model-aided inertial navigation for underwater vehicles. In: IEEE International Conference on Robotics and Automation, 2008. ICRA 2008. pp. 1069–1076 (2008)
8. Rigby, P., Pizzaro, O., Williams, S.: Towards georeferenced auv navigation through fusion of usbl and dvl measurements. In: OCEANS 2006, pp. 1–6 (2006)
9. Caruso, M.J.: Applications of magnetoresistive sensors in navigation systems. SAE Technical Paper 970602 (1997). doi:10.4271/970602. Link: http://papers.sae.org/970602/
10. "Compass heading using magnetometers," Application Note 203, Honeywell.
11. Vasconselos, J.F., Elkaim, G., Silvestre, C., Oliveira, P., Cardeira, B.: A geometric approach to strapdown magnetometer calibration in sensor frame. IEEE Trans. Aerosp. Electron. Syst. **47**(2), 1293–1306 (2008)
12. Fossen, T.I.: Guidance and Control of Ocean Vehicles, pp. 6–12. Wiley, Chichester, England (1994)
13. McPhail, S., Pebody, M.: Range-only positioning of a deep-diving autonomous underwater vehicle from a surface ship. IEEE J. Oceanic Eng. **34**(4), 669–677 (2009)
14. Philips, D.: An evaluation of usbl and sbl acoustic systems and the optimisation of methods of calibration—part 2. Hydrogr. J. **109**, 10–20 (2003)
15. Cooper, D.: System manual for fusion usbl navigation systems. User Manual, pp. 145–148 (2006)
16. Calibration and verification of sonardyne usbl systems: White paper (2009)
17. Snyder, J.: Doppler velocity log (dvl) navigation for observation-class rovs. In: OCEANS 2010, pp. 1–9 (2010)
18. Fossen, T.I.: Marine Control Systems, p. 57. Marine Cybernetics, Trondheim, Norway (2002)
19. Koh, T., Lau, M., Seet, G., Low, E.: A control module scheme for an underactuated underwater robotic vehicle. J. Intell. Robot. Syst. **46**(2), 43–58 (2006)
20. Sebastian, E., Sotelo, M.: Adaptive fuzzy sliding mode controller for the kinematic variables of an underwater vehicle. J. Intell. Robot. Syst. **49**, 189–215 (2007)
21. Refsnes, J.E., Sorensen, A.J.: Design of control system of torpedo shaped rov with experimental results. In: OCEANS '04, MTS/IEEE TECHNO-OCEAN '04, vol. 1, pp. 264–270 (2004)
22. Refsnes, J.E., Sorensen, A.J., Pettersen, K.Y.: Output feedback control of an auv with experimental results. In: Proceedings of the 15th Mediterranean Conference on Control & Automation, pp. 1–8 (2007)
23. Steinke, D., Buckham, B.: A kalman filter for the navigation of remotely operated vehicles. In: OCEANS, 2005. Proceedings of MTS/IEEE, vol. 1, pp. 581–588 (2005)
24. Fossen, T.I., Strand, J.P.: Passive nonlinear observer design for ships using lyapunov methods: experimental results with a supply vessel. Automatica **35**, 3–16 (1999)
25. Merhav, S.: Aerospace Sensor Systems and Applications, p. 396. Springer, New York (1996)
26. Alcocer, A., Oliveira, P., Pascoal, A.: Underwater acoustic positioning systems based on buoys with gps. In: Proceedings of 8th ECUA 06 (2006)
27. Gustafsson, F.: Adaptive Filtering and Change Detection. Wiley, New York (2000)
28. Blanke, M., Kinnaert, M., Lunze, J., Staroswiecki, M.: Diagnosis and Fault-Tolerant Control. Springer, Berlin Heidelberg (2010)
29. Basseville, M., Nikiforov, I.V.: Detection of Abrupt Changes: Theory and Application. Prentice-Hall, New York (1993)
30. Caccia, M., Bono, R., Bruzzone, G., Veruggio, G.: Bottom-following for remotely operated vehicles. Control Eng. Pract. **11**(4), 461–470 (2003)
31. Augenstein, S., Rock, S.: Estimating inertial position and current in the midwater. In: Proceedings of the MTS/IEEE Oceans Conference and Exhibition (2008)
32. Vaganay, J., Bellingham, J.G., Leonard, J.J.: Outlier rejection for autonomous acoustic navigation. In: Proceedings of IEEE Int. Conf. Robotics and Automation, pp. 2174–2181, (1996)
33. Menold, P.H., Pearson, R.K., Allgower, F.: Online outlier detection and removal. In: Proceedings of the 7th Mediterranean Conference on Control and Automation (MED99), pp. 1110–1133 (1999)
34. Jouffroy, J., Opderbecke, J.: Underwater navigation using diffusion-based trajectory observers. IEEE J. Oceanic Eng. **32**, 313–326 (2007)